NOT School - Project Report

Christian Cardin

University of Helsinki — January 18, 2024

Contents

1 Introduction **1**
1.1 Spectroscopy at the Nordic Optical Telescope 1
1.2 Project goals 2

2 Planning and observations **2**

3 Data **3**
3.1 FIESTool pipeline 4
3.2 Aggregation and cleanup 4

4 Correcting for Radial Velocity **5**

5 Spectrum Normalization **6**

6 Calculating R'_{HK} and R_o **7**

7 Estimating rotation velocity $v \sin i$ **7**

8 Comparison of emission lines **8**

9 Appendix: Source code **9**

NOTE: ChatGPT was used in this report for the production of text based on original work done by the Author. In particular, the AI has been used for proofreading, flow and cohesion improvements based on the original draft. Every picture and source code to generate the results are also original work from the Author.

1 Introduction

The study of young, magnetically active solar-type stars holds significant importance in advancing our understanding of stellar evolution and the underlying mechanisms driving stellar magnetic activity. Magnetic activity in stars, particularly in the form of surface features such as spots, flares, and prominences, is a complex phenomenon intimately linked to the star's rotation, magnetic field strength, and age. In this context, the present project focuses on utilizing the FIES high-resolution echelle spectrograph to conduct detailed astronomical observations of young solar-type stars, with the goal of studying their features.

1.1 Spectroscopy at the Nordic Optical Telescope

Spectroscopy, a fundamental tool in astrophysics, enables the analysis of celestial objects by dissecting their emitted or absorbed light into constituent wavelengths. The process involves the acquisition of a spectrum, a distribution of light intensity as a function of wavelength, which unveils valuable information about the physical and chemical properties of the observed astronomical targets. At the Nordic Optical Telescope (NOT), located on the island of La Palma, Spain, spectroscopic observations are conducted using the FIber-fed Echelle Spectrograph (FIES) [4]. This high-resolution instrument is equipped to capture detailed spectra across a broad wavelength range, making it particularly well-suited for studies requiring precision and sensitivity. The spectroscopic process at NOT involves the transmission of incoming light through a fiber-optic link from the telescope to FIES, where the echelle grating disperses the light into its component wavelengths, producing a high-resolution spectrum.

This dispersed light is then detected by a CCD sensor, allowing for the precise measurement of spectral lines and features.

1.2 Project goals

1. **Correction of Spectra for Radial Velocity (vrad):** The influence of stellar motion along the line of sight can introduce distortions in spectral features, and correcting for radial velocity is crucial for accurately interpreting these features for each other tasks of the project.

2. **Continuum Normalization for Regions of Interest:** Post-reduction, the 1D spectra retain a complex artificial continuum. The focus is on isolating and analyzing specific regions of interest by normalizing the spectra against a well-fitted continuum curve.

3. **Calculating log R'_{HK} and Comparing with Rotation:** The log R'_{HK} index serves as a key diagnostic for chromospheric activity. By calculating this index and comparing it with rotational parameters, we aim to discern correlations that shed light on the interplay between stellar rotation and magnetic activity. This analysis contributes to a broader understanding of how magnetic phenomena evolve in young solar-type stars.

4. **Comparing Line Profiles of Chromospheric Lines:** The investigation involves a detailed comparative study of line profiles associated with chromospheric lines. These spectral features offer insights into the complex magnetic activity occurring in the stellar atmospheres. By scrutinizing variations in line profiles across a sample of young solar-type stars, we aim to identify patterns and anomalies that provide a deeper understanding of magnetic phenomena.

5. **Estimating $v \sin i$:** This parameter not only aids in characterizing the rotational dynamics but also facilitates the separation of rotational effects from other stellar processes. The investigation into $v \sin i$ contributes to a comprehensive analysis of the stars' magnetic activity and its connection to rotation.

2 Planning and observations

Observations were performed on October 26^{th} 2023, a the Nordic Optical Observatory located at Roque de Los Muchachos, in La Palma (Spain).
We commenced our planning phase with the careful selection of targets from a pre-defined list. Each potential target underwent scrutiny based on criteria such as its visibility plot on the designated observation day and the altitude it would reach during our observation window, spanning from 19:30 to 01:00 local time in La Palma (Western European Time). The visibility plot for the selected targets is shown in Figure 1.
Moon presence was deemed inconsequential due to the substantial strength of starlight. This fortuitous circumstance allowed us to concentrate solely on optimizing our target list without the need to factor in lunar interference.
To ensure the acquisition of high-quality spectra, we calculated a suitable exposure time for each chosen target. The primary objective was to obtain a signal-to-noise ratio (SNR) of at least 90 in the CaII and R bandwidths. The parameters involved in the calculations were the airmass at the time of observation, approximate seeing conditions, star magnitude, and the number of exposures desired.
A noteworthy consideration in our exposure planning was the anticipation of cosmic ray-induced noise. Recognizing the potential impact of cosmic ray collisions with the detector, we strategically increased the number of exposures. This deliberate measure aimed at diminishing unwanted noise and enhancing the overall quality of the collected data. As we progressed through the planning phase, our efforts culminated in a refined strategy that maximized observational efficiency. The culmination of these meticulous preparations set the stage for the subsequent chapter, where we delve into the execution of our observational plan, detailing the selected targets and the outcomes of the spectroscopic observations conducted with the FIES instrument.
The following code snippet shows the commands that were used to setup the instrument, point the telescope and collect the data:

```
SCRIPT COMMAND ORDER:
############################
# Setup fies mode and observer for the whole session
$ tcs.setup-tel-fies
$ observer Helsinki2

# Append an object to be observed
$ tcs.append-object V889Her 18 34 20.1 +18 41 24.2 2000 0 0 7.45
```

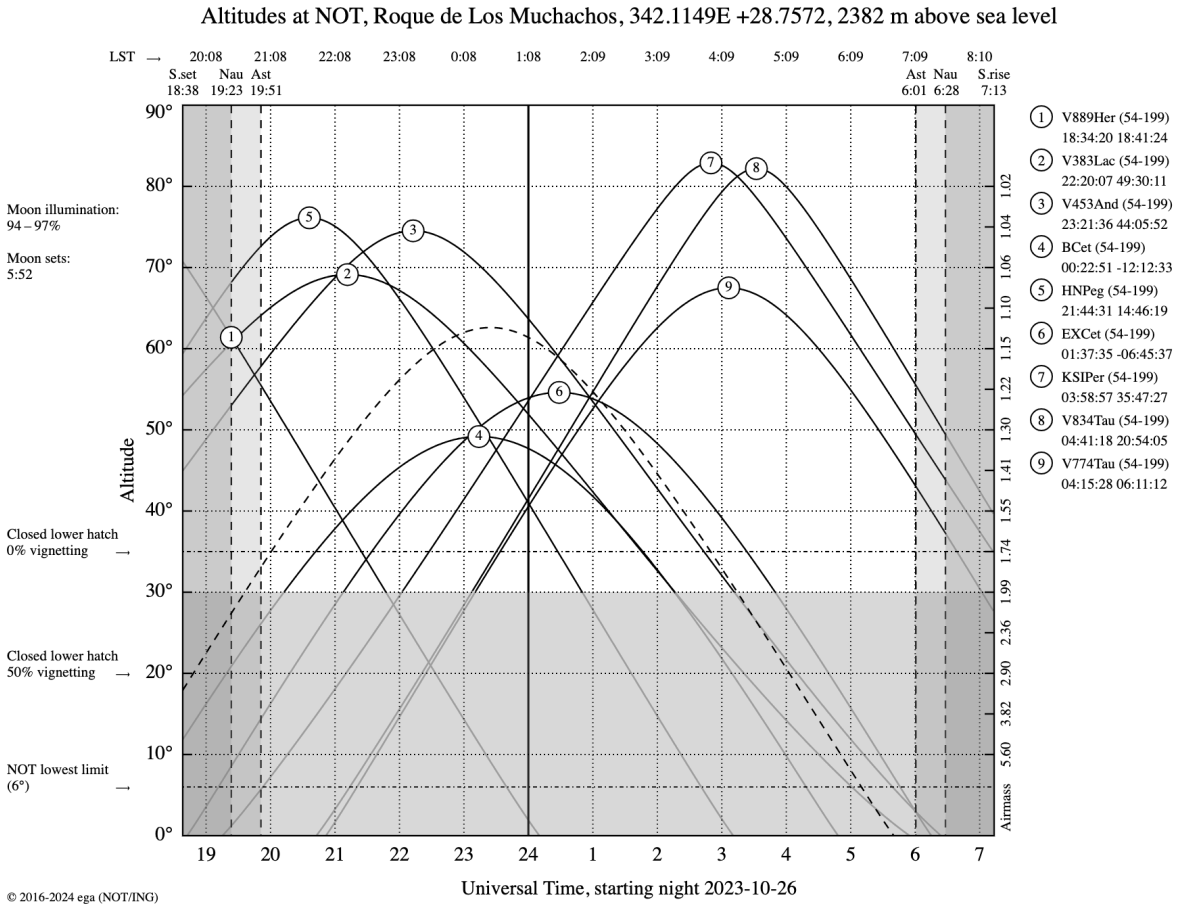

Figure 1: Visibility plot for selected targets

```
# Point the telescope
$ tcs.preset-with-parallactic-angle-to-selected

# Set object name
$ object V889Her

# Acquire target on fibre 4 (high-res) with 1s exposure (STANCAM sequencer)
$ acquisition 4 1

# Now, from the UI, find the object of interest, confirm the center of
# the star with the mouse.
# Then wait for fiber to align

# Take 3 exposures of 120s each
$ mexp 120 3

# Turn auto-guide off after the observation is done
$ tcs.ag-off

# Remember to kill movie mode sequence by moving on the UI panel
# and pressing ctrl-c
##############################
```

3 Data

The raw data consists of FITS images that capture the spectra of light as recorded by the sensor. Figure 2 provides a visual example of one such raw file, showcasing the complex information embedded within each spectral image.

Star	Mag	Time	Airmass	Exposure Time	S/N CaII	S/N R
V889Her	7.449	19:30 - 20:00	1.25	500s x 3 = 25m	99.75	202.77
V383Lac	8.61	20:00 - 21:00	1.1	1200s x 3 = 1h	92.65	185.11
V453And	7.37	21:00 - 22:30	1.05	400s x 3 = 20m	117.25	232.36
BCet	6.39	22:00 - 24:00	1.35	300s x 6 = 30m	182.81	364.23
HNPeg	6	22:00 - 23:00	1.1	400s x 3 = 20m	178.99	356.09
EXCet	7.67	23:00 - 24:00	1.35	800s x 3 = 40m	112.30	230.79
KSI Persei	4	23:30 - 24:00	1.5	300s x 3 = 15m	365.65	762.21
V774Tau	6.32	24:00 - 1:00	1.45	300s x 3 = 15m	126.15	262.17
V834Tau	8.06	24:00 - 1:00	1.4	700s x 3 = 45m	98.58	204.05

Table 1: Targets observation details

All raw files were made available in a shared online repository. In our data repository, each star is represented by three distinct FITS files, corresponding to the three exposures conducted for optimal signal-to-noise ratio. The data processing involves the use of the FIESTool pipeline, done at NOT, which converts the raw spectral images into a 1D representation in the frequency domain. This step simplifies the subsequent stages of data analysis and interpretation.

3.1 FIESTool pipeline

The reduction of echelle data can be a time-intensive process, diverting valuable time from the primary observational goals. This challenge is particularly pronounced when dealing with data from a new instrument, demanding a quick and efficient data reduction procedure. The FIESTool pipeline addresses this need, offering an automated solution for reducing data obtained with FIES at the Nordic Optical Telescope [3]. The key advantage of FIESTool lies in its ability to automatically reduce observations at the telescope, providing observers with a rapid first impression of the data. Automatic reduction also standardizes the reduction procedure and will simplify the user's effort by offering a default setup of reduction parameters.

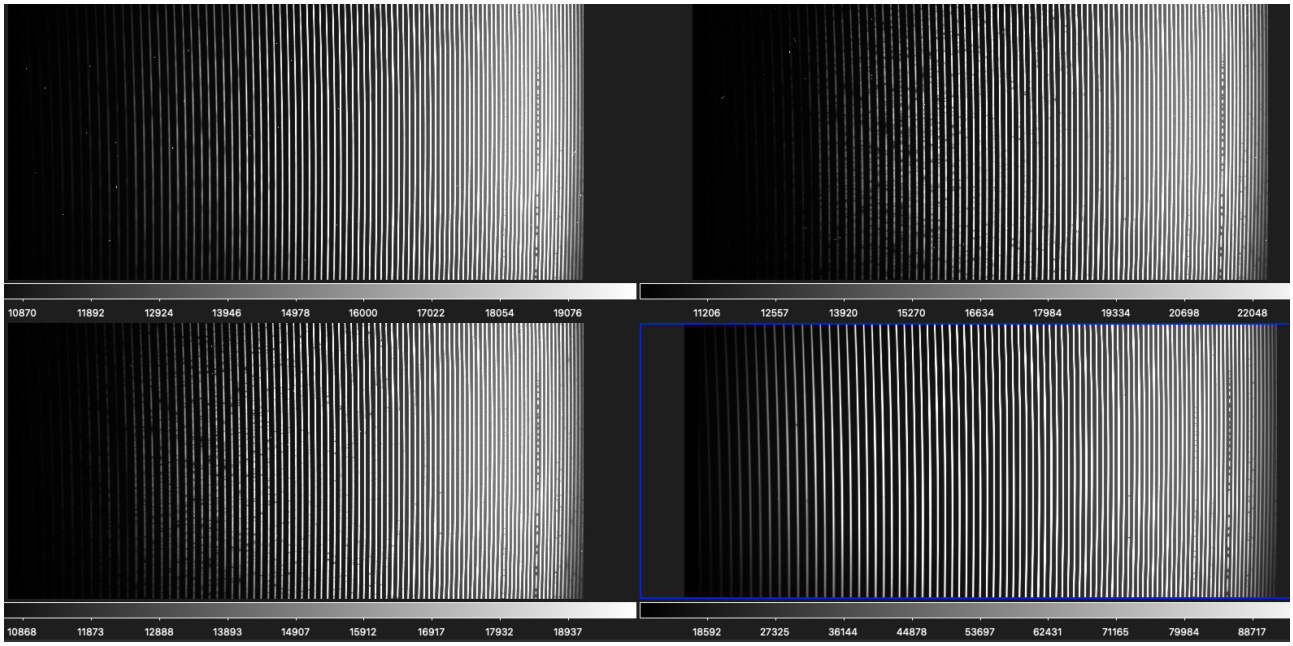

Figure 2: Raw spectra for, respectively, V889Her, BECet, V774Tau, KsiPer

3.2 Aggregation and cleanup

In the pre-processing phase of our data, the 1D spectra generated by the FIESTool output were subjected to an averaging process, enhancing the overall signal quality by consolidating information from multiple exposures. However, to refine the dataset further, it was necessary to address certain artifacts and sensor errors. Specifically, all negative values in the y-axis were systematically set to zero, a corrective measure that eliminated sensor anomalies. A visual representation of the effectiveness of these post-processing steps is depicted in Figure 3,

where residuals and relative errors from the mean of individual 1D spectra are showcased. This visual diagnostic tool provides insights into the success of our cleanup efforts and serves as a reference for the overall quality of the processed data.
Notably, specific regions in the spectra exhibited pronounced noise, particularly those at wavelengths less than 4000Å and around 7600Å, likely attributed to interferences such as internal reflections and diffractions induced by the optical fibers connecting the telescope to the CCD sensor. Although, the exact source of this interference needs further investigation.

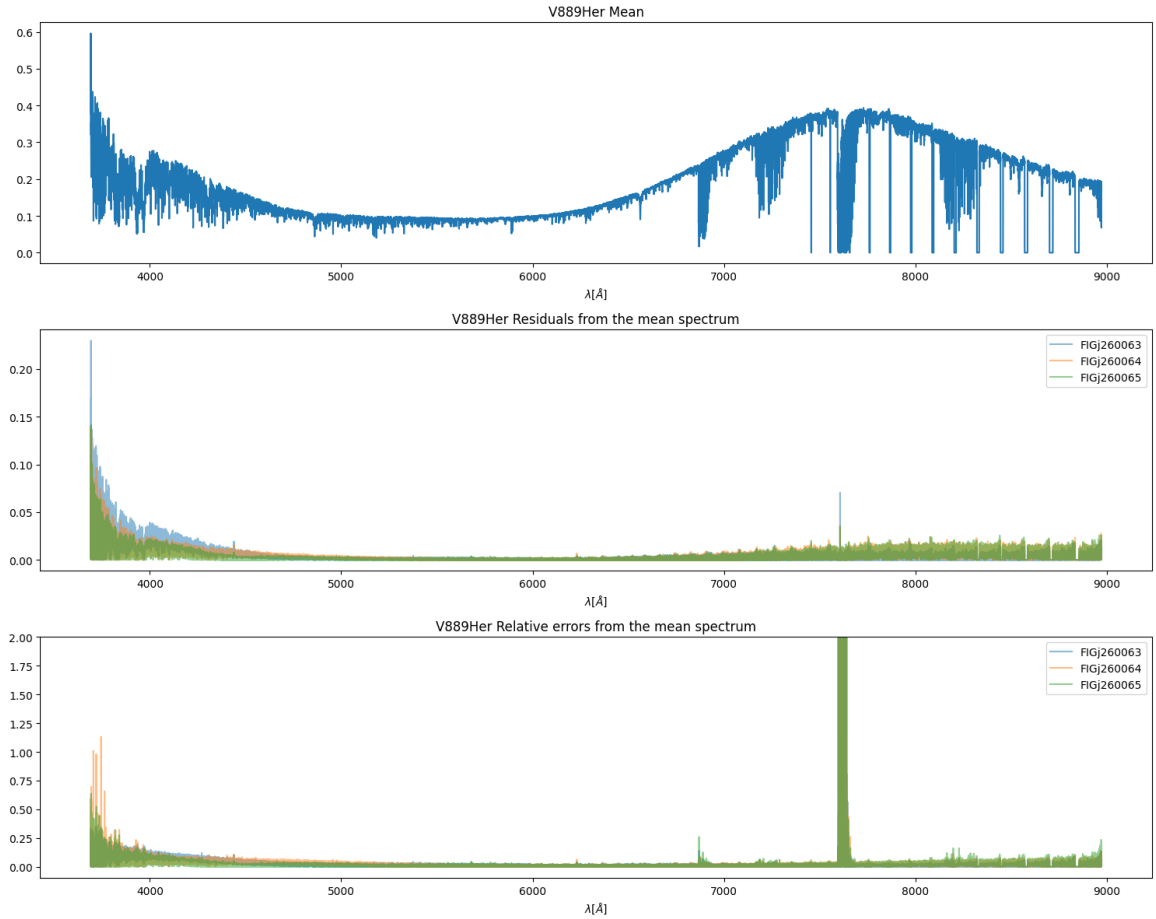

Figure 3: Reduced and aggregated spectrum of V889Her

4 Correcting for Radial Velocity

Achieving precision in astronomical spectroscopy demands careful consideration of redshifts induced by a star's motion relative to Earth. The impact of these redshifts on spectral features necessitates a correction, given by $\Delta\lambda = \frac{\lambda v_{\text{rad}}}{c}$, where c represents the speed of light, v_{rad} is the radial velocity, and λ denotes the wavelength of the measurement. The process of inferring v_{rad} from our data is a critical step in refining our spectroscopic observations. For this purpose, we pinpoint six specific wavelengths linked to metal absorption features (Table 2):

Wavelength (Å)	Element
5633.9458	Fe1
6024.0568	Fe1
6411.6476	Fe1
6430.8446	Fe1
6439.0750	Ca1
6643.6304	Ni1

Table 2: Absorption features considered

Star	v_{rad} **(km/s)**
BECet	-14.02
EXCet	-18.86
HNPeg	-7.36
V383Lac	10.77
V453And	-11.18
V774Tau	20.98
V834Tau	17.25
V889Her	1.95

Table 3: Radial Velocities (v_{rad}) for Different Stars

In the observed spectrum, the absorption dips deviate from the expected wavelengths, prompting the need for an accurate determination of v_{rad}. This determination involves finding the radial velocity that aligns each absorption dip with its anticipated wavelength. To achieve this alignment, we employ an optimization algorithm designed to minimize the Mean Absolute Error (MAE) between the original spectrum and its mirrored image around each feature line. To enhance the robustness of our radial velocity correction, we chose our final estimation based on the median value of all the estimations for individual emission lines. This choice is motivated by our observation that the optimization algorithm occasionally converges on incorrect values, introducing outliers that could significantly skew the average away from the true value. The median, being less sensitive to outliers, offers a more reliable measure for correcting the radial velocity in our spectroscopic data. After the determination of the optimal value for v_{rad}, shown in Table 3 the original star's spectrum is corrected. An example is shown in Figure 4.
Note that the Blue Giant star Xsi-Persei was left out from further analyses, because its spectrum was profoundly different from the others, and it would require a different approach than the other stars considered in this study.

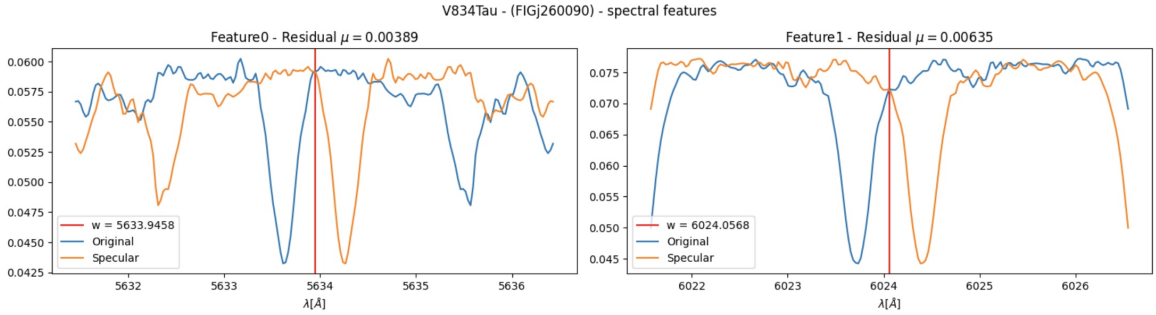

(a) Original spectrum with misaligned absorption dips

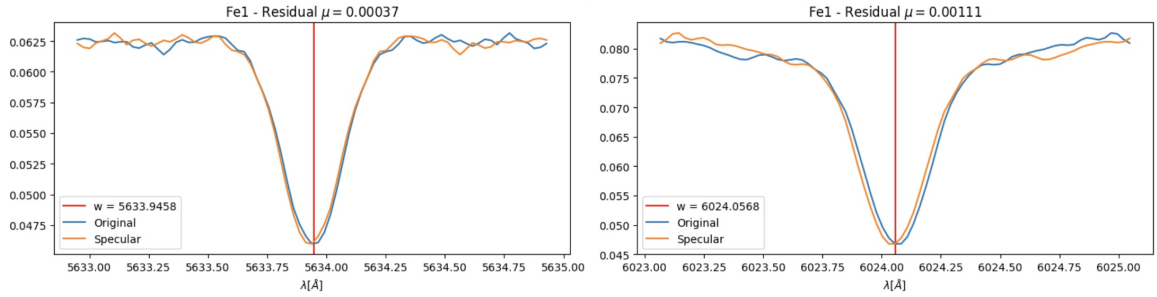

(b) Corrected spectrum with aligned absorption dips

Figure 4: Example of radial velocity correction

5 Spectrum Normalization

Spectrum normalization is an essential preprocessing step in spectroscopy, addressing challenges associated with the artificial continuum introduced by CCD detector sensitivity. The primary objective is to flatten the continuum in specific spectral regions, enhancing the accuracy of subsequent analyses, such as the calculation of chromospheric excess emission.
The normalization process employs an iterative algorithm, consisting of the following steps:

1. Fit a curve to a designated region using a polynomial of a suitable degree.
2. Divide the spectrum by the fitted curve.
3. Remove data points below the mean intensity of the resulting spectrum.
4. Repeat the process until spectral peaks are appropriately aligned.

For testing and optimization purposes, a specific spectral slice between 3875Å and 4025Å was considered. In our implementation, we conducted eight iterations using a fourth-degree polynomial for the majority of stars. However, recognizing variations in specific cases, we adjusted the parameters for certain stars. For example, for V834Tau, we reduced the iterations to three and the polynomial degree to three. In the case of V383Lac, five iterations were performed using a third-degree polynomial.

An illustrative example of the spectrum normalization process is depicted in Figure 5. This figure showcases the effectiveness of the iterative algorithm in achieving a flattened continuum in the designated spectral region. The refined spectra resulting from the normalization process provide a more reliable basis for subsequent analyses.

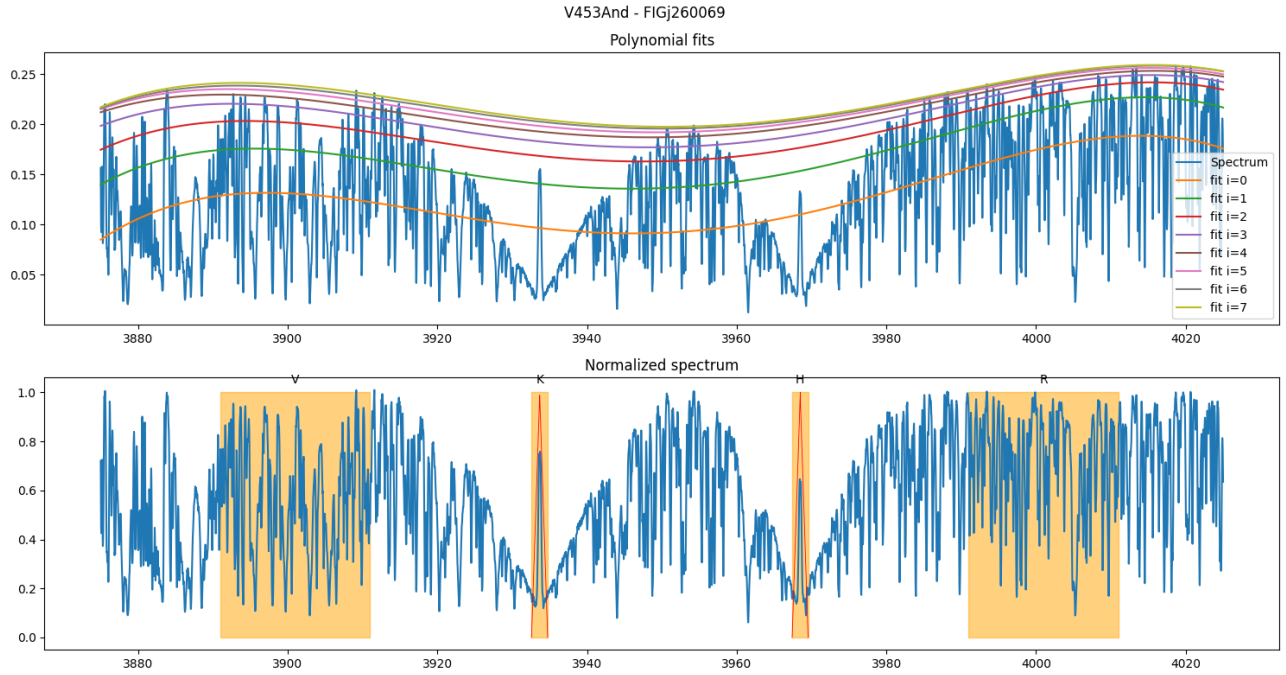

Figure 5: Spectrum normalization for star V453Lac. Each colored line represent a subsequent polynomial fit.

6 Calculating R'_{HK} and R_o

Stellar magnetic activity can be assessed using chromospheric excess emission in the Ca II H and K lines, which reflect the magnitude of a star's magnetic fields. This emission is quantified by the R'_{HK} index, a measure of the flux emitted per unit stellar surface area after accounting for an inactive photosphere.
The R'_{HK} index provides insights into the stellar age, metallicity, and rotation rate, with high activity levels typically corresponding with younger, more metallic, or faster-rotating stars. Another parameter, the Rossby number (R_o), defined as the ratio of the star's rotation period to its convective turnover time ($R_o = P_{rot}/\tau_c$), also serves to gauge a star's magnetic activity. R_o investigates the impact of the rotation rate on magnetic activity. By plotting log R'_{HK} against log R_o, a rotation–activity relationship emerges in which faster rotation (smaller R_o) corresponds with higher activity (greater R'_{HK}). This relationship quantifies the influence of rotation on magnetic activity, and a plot for the considered stars is shown in Figure 6.
R'_{HK} is computed based on the S-Index (S = $\alpha \frac{H+K}{R+V}$) where H, K, R, and V refer to the integrals of the normalized spectra of the corresponding bands highlighted in Figure 5. $\alpha = 19.76$ is a constant term.
In order to properly calculate the area under the curve for the H, K, V, R bands, the spectrum needs to be normalized as described in Section 5. The normalization process uses a region between 3875Å and 4025Å. Additionally, R and V must undergo additional normalization using a triangular function. This function intensifies their contribution at the band center while minimizing the contributions at the band edges.
Computing the integral numerically is achieved using the `np.trapz()` function from the Numpy library. For a more comprehensive understanding of this computation, please visit the repository containing the pertinent source code (See Section 9)

7 Estimating rotation velocity $v \sin i$

Stellar rotation causes a broadening of spectral lines due to Doppler shifts across the stellar surface. In our study, we focus on estimating the rotation velocity denoted by $v \sin i$, where v represents the equatorial rotational velocity, and i is the inclination angle of a star's rotation axis to the line of sight. This parameter is important as it captures the projected rotational velocity, influenced by both the actual velocity and the observer's viewing angle.

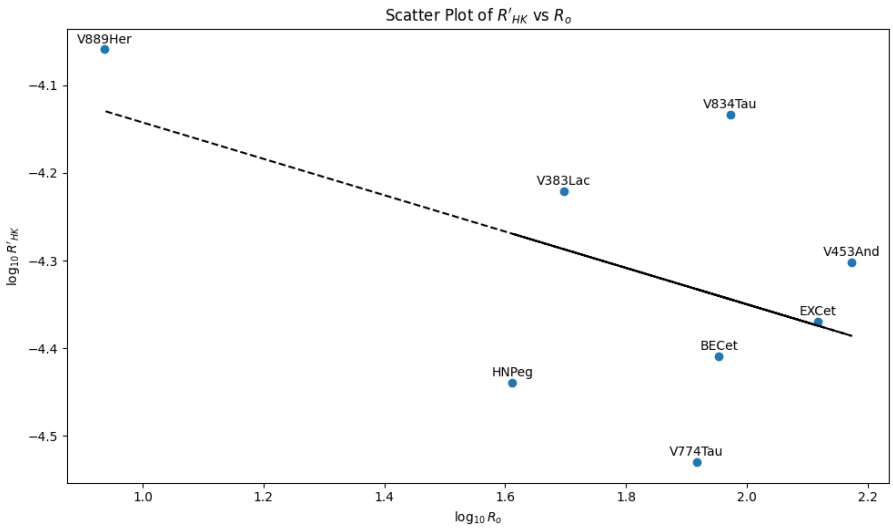

Figure 6: Star Activity vs Rotation relationship. Smaller R_o indicates higher activity

To derive $v \sin i$, we used a numerical approach similar to the one employed for estimating v_{rad}. Our methodology involved selecting a specific interval centered around the metal line at 6024.0568, a region devoid of significant noise across all considered stars (See Figure 7a). Min-max normalization was applied to the spectra before the fitting, thus regularizing the algorithm and increasing the chances of convergence to the real estimation.

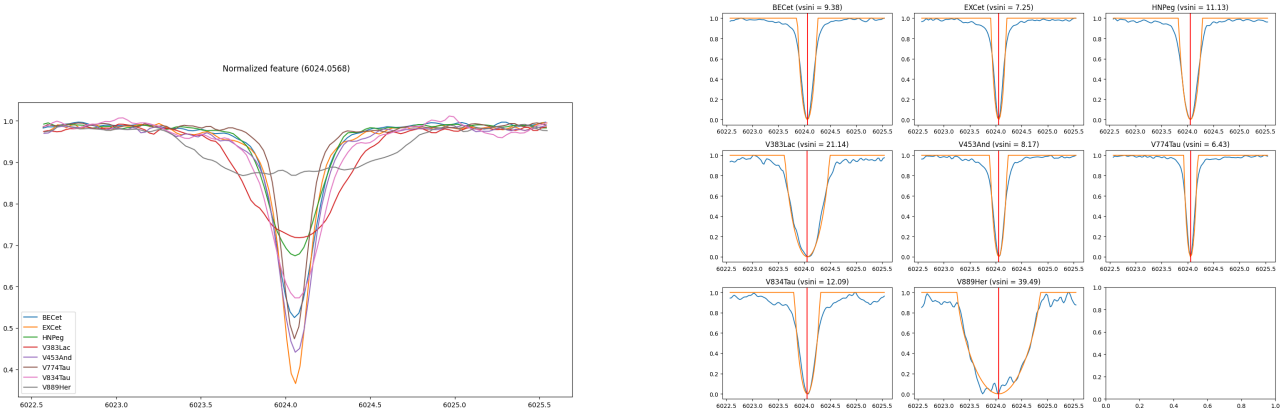

(a) Comparison of broadened lines at $w = 6024.0568$

(b) Fitted curve to broadened lines

Figure 7

For each individual star, a curve [1], incorporating $v \sin i$ as a latent parameter, was fitted to the rotationally broadened line. In Figure 7b there's a visualization of the fitted polynomial. The objective was to minimize the Mean Absolute Error (MAE), providing a robust foundation for accurate estimations. The outcomes of this numerical exploration are encapsulated in Table 4, presenting the obtained $v \sin i$ values for each star.
A critical aspect of our analysis involved a comparison with literature values [2], illustrated in Figure 8. Intriguingly, our method consistently demonstrated a tendency to overestimate $v \sin i$ values compared to those from existing literature.

8 Comparison of emission lines

In addition to the prominent Ca II H&K lines, the chromosphere of stars exhibits strong emission components in other spectral lines such as the $H\alpha$ line and the Ca II infrared triplet (IRT) lines. Unlike the Ca II H&K lines, there is a lack of standardized methods for precisely measuring the core emission of these lines. Specifically, for $H\alpha$, accurate measurements necessitate the subtraction of the correct absorption profile.
While a standardized approach for measuring these lines remains elusive, qualitative comparisons can still be made by examining line profiles or depths. For $H\alpha$, an additional metric for analysis is the calculation of the equivalent width, offering insights into the extent to which the absorption profile is filled in by the emission.

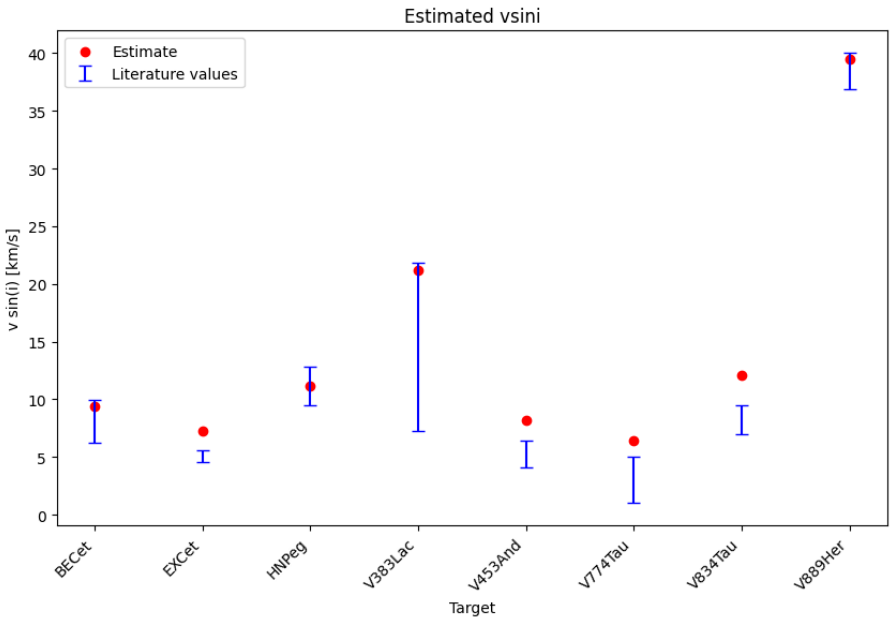

Figure 8: Comparison with literature values

Star	$v \sin i$ [km/s]
BECet	9.38
EXCet	7.24
HNPeg	11.13
V383Lac	21.15
V453And	8.17
V774Tau	6.43
V834Tau	12.09
V889Her	38.89

Table 4: Estimated $v \sin i$ values.

Following the normalization of the spectrum, the implementation of code facilitates the plotting of the surroundings of interesting spectral features. This qualitative comparison was executed for each star around the lines Ca II K, Ca II H, $H\alpha$, and Ca II IRT, corresponding to wavelengths 3933.66, 3968.47, 6562.8, 8498, 8542, and 8662 Å, respectively.
This comparative analysis was conducted for each star, producing plots of the spectral features around Ca II K, Ca II H, $H\alpha$, and Ca II IRT. As an illustrative example, Figure 9a and Figure 9b showcase these plots for two selected stars, namely V889Her and BECet. These visual representations offer a nuanced understanding of the qualitative variations in the line profiles of different stars across various chromospheric lines.

9 Appendix: Source code

The source code used for data exploration and parameter estimation can be found in the Helsinki University GitLab server, at the address https://version.helsinki.fi/ccardin/astro_obs_2023.
To run the code, a Python version 3.10+ is recommended. The project includes 6 Jupyter Notebooks that showcase each goal. Also, a *pipeline.py* file serves as a convenient entry point which automatically downloads the FITS data, processes them and stores the results under the `out/` folder. To run it, simply execute:

```
git clone https://version.helsinki.fi/ccardin/astro_obs_2023.git
cd astro_obs_2023
pip install -r requirements.txt
cd spectroscopy
python pipeline.py
```

References

[1] Diaz, C. & Gonzalez, Jorge & Levato, Orlando & Grosso, M.. (2010). Accurate stellar rotational velocities using the Fourier transform of the cross correlation maximum. Astronomy & Astrophysics - ASTRON ASTROPHYS. 531. 10.1051/0004-6361/201016386.

[2] Simbad Database. https://simbad.cds.unistra.fr/simbad/

[3] FIEStool at NOT telescope. https://www.not.iac.es/instruments/fies/fiestool/FIEStool.html

[4] Telting, J. H., "FIES: The high-resolution Fiber-fed Echelle Spectrograph at the Nordic Optical Telescope", Astronomische Nachrichten, vol. 335, no. 1, p. 41, 2014. doi:10.1002/asna.201312007.

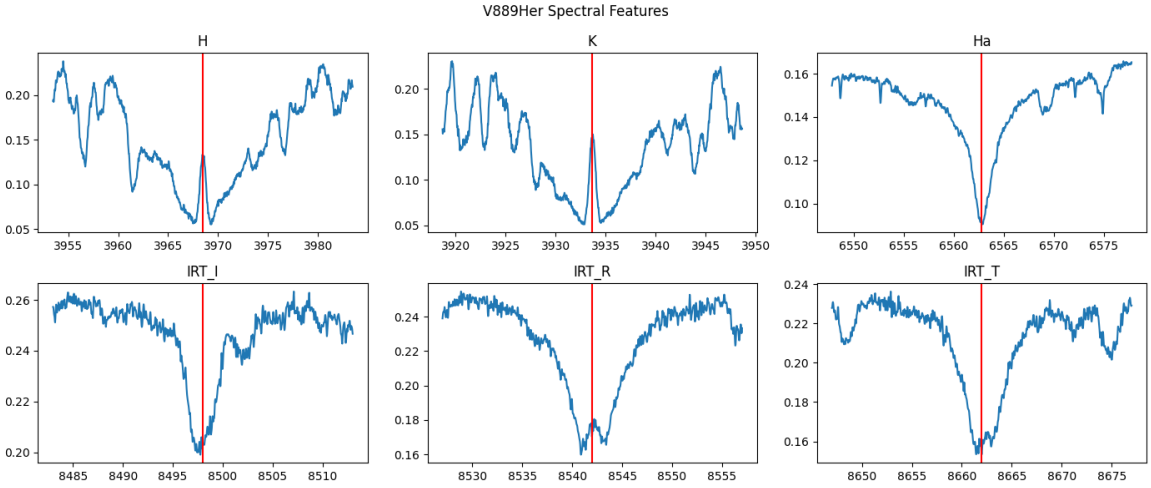

(a) Features of V889Her

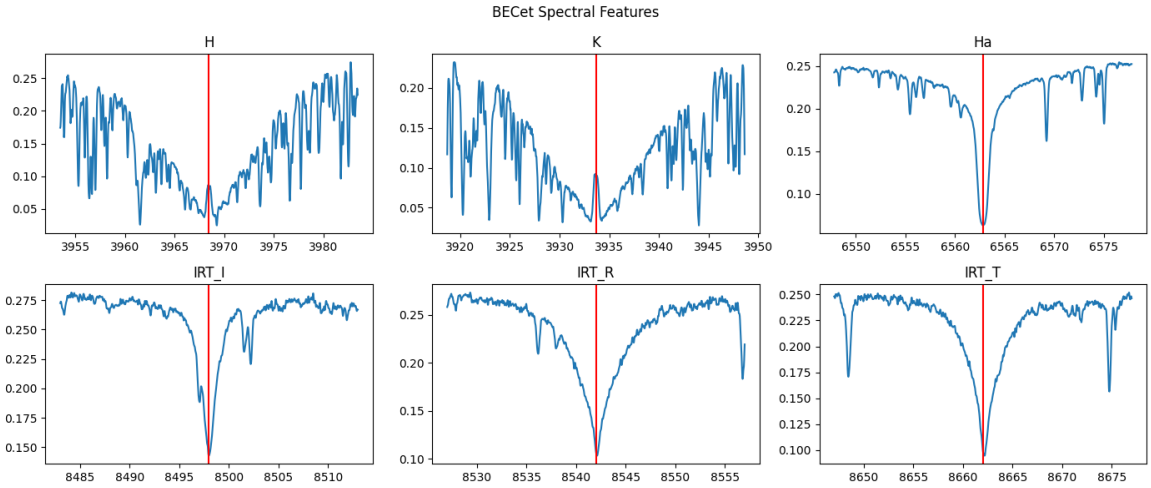

(b) Features of BECet

Figure 9: Comparison of Chromospheric Line Features